International Journal of Mass Spectrometry 273 (2008) 11–19

Contents lists available at ScienceDirect

International Journal of Mass Spectrometry

journal homepage: www.elsevier.com/locate/ijms

A theoretical and mass spectrometry study of the fragmentation of mycosporine-like amino acids

Karina H.M. Cardozo[a,b,1], Ricardo Vessecchi[c,1], Valdemir M. Carvalho[d], Ernani Pinto[e], Paul J. Gates[b], Pio Colepicolo[a], Sérgio E. Galembeck[c,*], Norberto P. Lopes[f,*]

[a] *Departamento de Bioquímica, Instituto de Química de São Paulo, Universidade de São Paulo, Av. Professor Lineu Prestes, 748 CP 20780, CEP 05508-900, São Paulo-SP, Brazil*
[b] *School of Chemistry, University of Bristol, Cantock's Close, Bristol, BS8 1TS, United Kingdom*
[c] *Departamento de Química, Faculdade de Filosofia, Ciências e Letras de Ribeirão Preto, Universidade de São Paulo, Av. dos Bandeirantes 3900, CEP 14040-901, Ribeirão Preto-SP, Brazil*
[d] *Instituto Fleury, Av. General Waldomiro de Lima, 508 CEP 04344-070, São Paulo-SP, Brazil*
[e] *Departamento de Análises Clínicas e Toxicológicas, Faculdade de Ciências Farmacêuticas - São Paulo, Universidade de São Paulo, Av. Professor Lineu Prestes, 580 CEP 05508-900, São Paulo-SP, Brazil*
[f] *Departamento de Física e Química, Faculdade de Ciências Farmacêuticas de Ribeirão Preto, Universidade de São Paulo, Av. do Café, CEP 14040-903, Ribeirão Preto-SP, Brazil*

ARTICLE INFO

Article history:
Received 12 June 2007
Received in revised form 11 February 2008
Accepted 11 February 2008
Available online 29 February 2008

Keywords:
Mycosporine-like amino acids
Natural products
High-resolution mass spectrometry
Theoretical calculations
Radical elimination
Algae

ABSTRACT

In the present study, the mycosporine-like amino acids (MAAs) were isolated from the marine red alga *Gracilaria tenuistipitata* and analysed by high-resolution accurate-mass sequential mass spectrometry (MS^n). In addition to the proposed fragmentation mechanism based on the MS^n analysis, it is clearly demonstrated that the elimination of mass 15 is a radical processes taking place at the methoxyl substituent of the double bond. This characteristic loss of a methyl radical was studied by theoretical calculations and the homolytic cleavage of the O—C bond is suggested to be dependent on the bond weakening. The protonation site of the MAAs was indicated by analysis of the Fukui functions and the relative Gibbs energies of the several possible protonated forms.

1. Introduction

Amongst the diversity of methods used by organisms to reduce damage caused by ultraviolet (UV) radiation, the synthesis of UV-screening compounds is almost universal. One class of sunscreen compounds that has been discussed in several papers [1–4] are the substances called mycosporine-like amino acids (MAAs). These compounds, which are present intracellularly in many marine and fresh-water algae and phytoplankton [4–6], are characterised by an aminocyclohexenone or aminocyclohexenimine ring with nitrogen or imino alcohol substituents (Fig. 1). Their strong UV absorption maxima between 310 and 360 nm and high molar extinction coefficients sustain the hypothesis of a photoprotective role that has been demonstrated in a number of studies [7–9]. In addition to a UV protective function, it has been suggested that MAAs also have antioxidant activity [10], osmotic functions [11], and a regulatory role in reproduction [12]. Regarding their applications, they have been commercially explored as sunscreen products for skin protection and for protection of non-biological materials as photostabilising additives in the plastics, paint and varnish industries [1,13]. To date, around 20 MAAs have been characterised and identified in aquatic environments [14].

Because of their scientific and commercial interest, several academic research groups and cosmetic companies started to study the structural elucidation of these compounds using electrospray tandem mass spectrometry (ESI–MS/MS), but the characterisation and quantification of MAAs is typically performed by high performance liquid chromatography (HPLC) along with UV detection. A diode array detector (DAD) that allows the acquisition of spectral data is the most applied technique [15,16]. A recent study published an HPLC method based upon use of reverse-phase C_{18} columns with

* Corresponding authors. Tel.: +55 16 3602 4707; fax: +55 16 3602 4243.
E-mail addresses: segalemb@usp.br (S.E. Galembeck), npelopes@fcfrp.usp.br (N.P. Lopes).
[1] This study was conducted as a part of the PhD research.

1387-3806/$ – see front matter © 2008 Elsevier B.V. All rights reserved.
doi:10.1016/j.ijms.2008.02.014

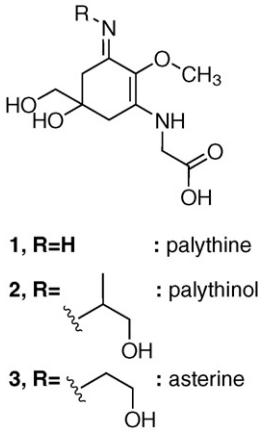

Fig. 1. Structures of the three mycosporine-like amino acids (MAAs) analysed.

trifluoroacetic acid/ammonium as the mobile phase that separated a mixture of over 20 MAAs with good selectivity for high, medium and low polarities [14]. Besides HPLC methods, several mass spectrometric methods of analysis have also been applied [17–19]. The increased application of mass spectrometry to the analysis of natural products is related to the increased quality of the structural information furnished by elucidation of fragmentation patterns [20–22]. However, for full structure-elucidation, it is necessary to understand all the gas-phase chemistry involved in each fragmentation step and to clarify the relationships between all the different possible pathways [22]. In addition, the analysis of natural product extracts is normally hampered by the absence of commercially available standards. Since the total structural diversity of this class of compounds remains unknown, more information is necessary for the precise identification of MAAs discovered in different aquatic organisms.

Previous reports focusing on the fragmentation patterns of some MAAs showed a loss of mass 15 when analysed by positive mode low-resolution ESI–MS/MS [19]. It was also demonstrated that this loss was not an artifact of the technique by performing further studies with low resolution MS^3 [19]. It has been suggested, based on observations resulting from the analysis of polyamines in ion-trap mass analysis [23], that this small loss could be due to elimination of a methyl radical. The authors emphasised that further work was necessary to comprehend and prove the formation of this radical [19]. For palythine, it was also suggested that loss of mass 15 could be due to elimination of NH, but previous studies with triple quadrupole MS/MS dispute this suggestion [24]. Recently, the fragmentation by collision-induced dissociation (CID) MS/MS of protonated peptides and α-amino acids at high collision energies, showed eliminations of small radicals including $H^{\bullet}$, $^{\bullet}CH_3$ and $NH{=}CH^{\bullet}$ [25]. Though the occurrence of these radical fragments has been evidenced in the literature, studies of the bond reinforcement or weakening after protonation will help to understand the fragmentation process. Using AIM theory [26] the character of these bonds can be analysed. It has been shown that the bonding perturbation caused by protonation depends on the center to which the proton is attached [27]. Thus, the search for the protonation site becomes an important first step for the elucidation of the possible unimolecular mechanistic pathways.

Based upon these previous studies, the purpose of this work is to establish a sound basis for the mechanism of the fragmentation of MAAs and to explain the possible methyl radical elimination by using high-resolution accurate-mass MS^n along with theoretical calculations.

2. Experimental

2.1. Chemicals

All solvents used were HPLC grade (Tedia, J. Baker and Fisher). Water was purified using a Milli-Q system (Millipore, Bedford, MA, USA). Trifluoroacetic acid (99.9%) was purchased from Aldrich and Sephadex LH-20 from Sigma.

2.2. Algal material

Cultures of the marine red macroalga *Gracilaria tenuistipitata* Chang et Xia (Gracilariales, Rhodophyta) were grown in von Stosch medium [28] under alternating periods of 12 h light (cool white fluorescent; 120 $\mu E\,m^{-2}\,s^{-1}$) and 12 h dark (LD 12:12). The cultures were maintained at 20 °C under constant air bubbling. Algae were harvested in the middle of the light period. Samples were frozen in liquid nitrogen and kept at −80 °C until the extraction of the MAAs was performed.

2.3. Extraction of the MAAs

About 600 g of frozen *G. tenuistipitata* was homogenised and extracted with methanol:water (1:1) at 4 °C for 24 h (4× 600 mL). After centrifugation (10,000 rpm for 10 min at 4 °C) the supernatant (1/3 of total) was lyophilised and the extract (14.5 g) was suspended in ≅30 mL of methanol. The supernatant was collected and dried. The content of this fraction (1.4 g) in methanol was applied to a Sephadex LH-20 column (80 cm × 5.0 cm) using methanol as eluent (flow rate 2.4 mL min^{-1}). Fractions were pooled after the HPLC analyses as previously described [14] with few modifications. The fraction containing palythine and its derivatives was selected and purified by semi-preparative HPLC.

2.4. Instrumentation

Accurate-mass MS^n analyses were performed on an Apex IV (7 Tesla) Fourier-transform ion cyclotron resonance instrument (FTICR) (Bruker Daltonics, Billerica, MA, USA). Solutions were infused by syringe pump through the Apollo ESI source at 100 $\mu L\,h^{-1}$. Fragmentation analyses were performed on the isolated parent ions by sustained off-resonance irradiation collision induced dissociation (SORI-CID) using CO_2 collision gas. Precursor ions were selectively isolated through correlated sweep isolation with a short period of collisional cooling after isolation. In some cases, a novel technique termed "double isolation" was required to isolate the precursor ions—this is when a second isolation step is used to separate the desired precursor ions from unwanted isobaric impurites. Sequential fragmentation steps were performed on optimised precursor ions from the previous step. The ESI spectra and isolation experiments were performed at a resolution of approximately 50,000 and the MS^n spectra had a resulting resolution of approximately 80,000. Usually 8 or 16 individual scans were combined to produce a spectrum. On some occasions (when the signal was very weak), as many as 40 scan summations were required to produce spectra with a good signal:noise ratio. An accurate-mass calibration was obtained for all sequential mass spectrometry spectra through use of a pre-calibrated experiment file resulting from the MS/MS of a known standard achieved under the same CID and cell conditions. Mass-accuracies were well within 1 ppm of the theoretical masses for most ions observed.

2.5. Theoretical calculations

All calculations were made with the B3LYP/6-31 G + (d, p) model [29,30], using the Gaussian 98 suite of programs [31], in the gas-

phase, to mimic the environment of CID-MS/MS as closely as possible. The geometries of the neutral and protonated molecules were fully optimised and the vibrational frequencies analysis indicates that all structures are minima in the potential energy surface. The electron density was analysed by Natural Resonance Theory (NRT) [32,33], Natural Bond Orbitals (NBO) [34,35] and Natural Population Analysis (NPA) [36] methods, with NBO 5.0 software, interfaced in Gaussian 98. Topological analyses of the charge densities (ρ_b) and their Laplacian (∇^2) were made by the Atoms in Molecules method [26,37], using AIM 2000 [38]. The bond critical point (BCP) between two atoms assures the existence of some bonding between them. The value of the charge density at this critical point is a measure of the strength of the linkage.

Our studies were based on the AIM method and the analyses of the wave function for the neutral and protonated molecules focused on the reinforcement or weakening of the O—CH_3 bond. The most probable protonation sites for the neutral molecule were determined through analysis of the Fukui functions [39] and relative Gibbs energies between the possible protonated species.

3. Results and discussion

3.1. Protonation site on MAAs and formation of $[(M+H)-15]^+$ ion

The selected fraction was submitted to semi-preparative HPLC and yielded palythine, palythinol and asterina (Fig. 1), in addition

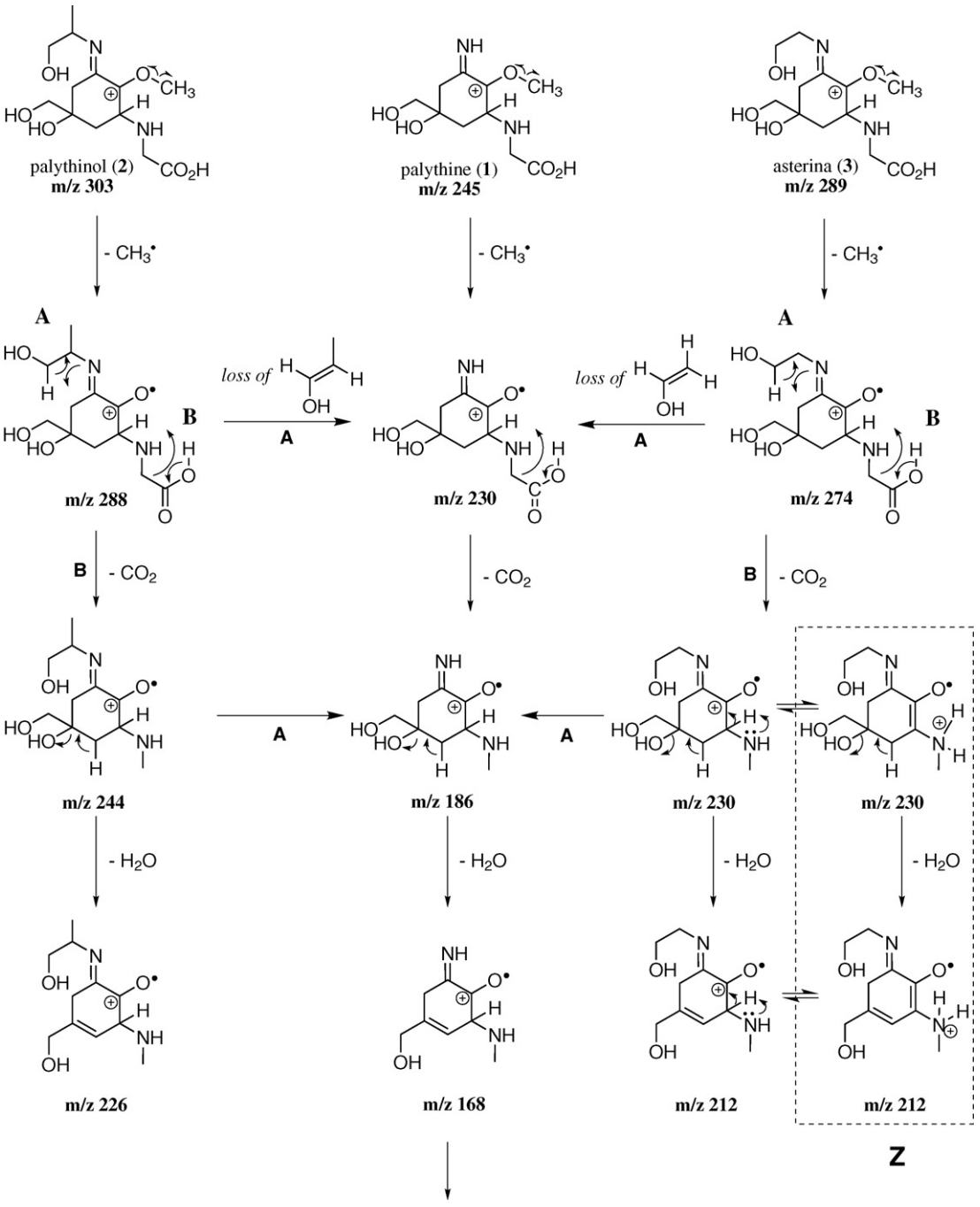

Scheme 1. The homolytic bond cleavage to produce the loss of the methyl radical and the proposed mechanism of the subsequent radical cation fragmentation for the three MAAs analysed. The order of pathway A may change at different energies. After the CH_3 radical elimination the product ions may keep the protonation site at the double bound or relocate the proton through the equilibrium suggested in the box labelled 'Z'.

Table 1
A summary of the accurate-mass ESI–FTICR-MS^n data for the fragmentation of palythinol

Ion	Formula	Theoretical mass	Observed masses (ppm error)				
			MS/MS	MS^3 (288)	MS^3 (244)	MS^3 (230)	MS^3 (186)
$[M+H]^+$	$C_{13}H_{23}N_2O_6^+$	303.15506	303.15505 (−0.03)				
303, $CH_3^\bullet$	$C_{12}H_{20}N_2O_6^{\bullet+}$	288.13159	288.13151 (−0.28)	288.13158 (−0.03)			
288, CO_2	$C_{11}H_{20}N_2O_4^{\bullet+}$	244.14176	244.14174 (−0.08)	244.14177 (+0.04)	244.14176 (0)		
303, CO_3H_8	$C_{12}H_{15}N_2O_3^+$	235.10772	235.10770 (−0.09)	–	–		
288, C_3H_6O	$C_9H_{14}N_2O_5^{\bullet+}$	230.08972	230.08985 (+0.56)	230.08973 (+0.04)	–	230.08971 (−0.04)	
244, H_2O	$C_{11}H_{18}N_2O_3^{\bullet+}$	226.13119	226.13122 (+0.13)	–	226.13120 (+0.04)	–	
303, $C_4H_{10}O_3$	$C_9H_{13}N_2O_3^+$	197.09207	197.09209 (+0.10)	197.09208 (+0.05)	197.09215 (+0.41)	–	
230, CO_2	$C_8H_{14}N_2O_3^\bullet$	186.09989	186.09989 (0)	186.09988 (−0.05)	186.09986 (−0.16)	186.09990 (+0.05)	186.09988 (−0.05)
186, H_2O	$C_8H_{12}N_2O_2^\bullet$	168.08933	–	–	–	–	168.08935 (+0.12)
186, $CH_3O^\bullet$	$C_7H_{11}N_2O_2^\bullet$	155.08150	–	–	–	–	155.08148 (−0.13)
168, $OH^\bullet$	$C_8H_{11}N_2O^+$	151.08659	–	151.08661 (+0.13)	–	–	151.08662 (+0.20)
168, H_2O	$C_8H_{10}N_2O^{\bullet+}$	150.07876	150.07870 (−0.40)	150.07876 (0)	150.07878 (+0.13)	150.07861 (−1.00)	150.07876 (0)
155, NH_3	$C_7H_8NO_2^{\bullet+}$	138.05495	–	–	–	–	138.05478 (−1.23)
155, H_2O	$C_7H_9N_2O^+$	137.07094	137.07097 (+0.22)	137.07094 (0)	137.07093 (−0.07)	137.07094 (0)	137.07094 (0)

The formulae, identities, theoretical masses and observed masses (with ppm mass error in parenthesis) are listed for all major product ions observed.

to several sugars and other biological compounds not discussed further here. High-resolution accurate-mass tandem mass spectrometry of all compounds confirmed the elimination of a CH_3 radical (Scheme 1 and Table 1) and ruled out any possibility that elimination of NH was occurring, as had previously been suggested [19]. Based on these results, we considered the CID-MS/MS energy (kinetic energy transfer) to be sufficient to induce the unimolecular dissociation (by the presence of the $[(M+H)\text{-}15]^+$ product ion). In this case, the difference between the initial and final energy states can be used to understand the mechanism and it is not necessary to consider the energies of any transition species. On this basis, the theoretical calculations were for the energy necessary for the cleavage of the ether bond after the protonation (as proved by high resolution FTICR–MS) and also for the variations in the electronic density for all species. The chemistry of ions in the gas-phase may be thought of as an ideal process since the ions can be considered to be isolated. In this context, the methodologies that are used to solve the Schrödinger equation (either *ab initio* or DFT) apply the condition of the absence of any intermolecular interactions [40–43].

The protonation site of palythine was obtained by the analysis of the electrophilic Fukui function, f^-, which is found to be higher at the C(7) atom, followed by N(8), N(2) and C(6) atoms (Fig. 2 and Table 2). Similar results were observed for palythinol and asterina. The structure of the palythine cations protonated at C(6), C(7), N(8) and N(2) were fully optimised by using of B3LYP/6-31 + G(d, p) model (Fig. 3). In order to understand the role of resonance on the cleavage of the O—CH_3 bond in the MAAs, parameters such as bond length, relative Gibbs energies and charge density between the neutral and protonated molecules were compared.

Several structural differences can be observed upon comparing the protonated species and neutral molecule, such as an increase in the O(14)—C(15) bond length after protonation (Table 3). This is the initial evidence for weakening of the O—CH_3 bond after pro-

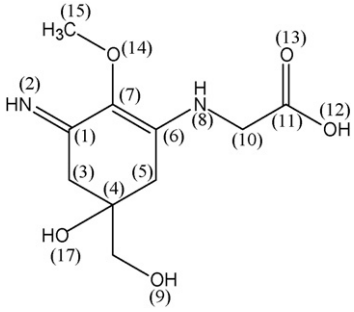

Fig. 2. The structure of palythine and the atom labels used for the Fukui function analyses.

Table 2
Values of atomic Fukui functions indicating the most probable sites of protonation

Atom number	f^-
C(1)	−0.014699
N(2)	0.175412
C(3)	0.004007
C(4)	0.045686
C(5)	−0.016329
C(6)	0.168873
C(7)	0.323334
N(8)	0.199601
O(9)	0.000221
C(10)	0.019869
C(11)	0.002960
O(12)	0.015822
O(13)	0.003871
O(14)	0.039660
C(15)	0.009687
C(16)	−0.015893
O(17)	0.002450

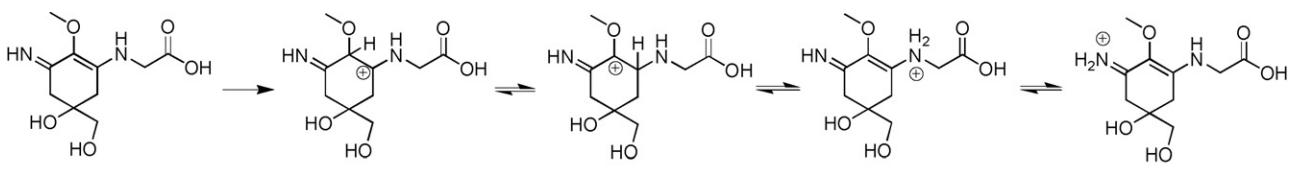

Fig. 3. Structure of protonated species for palythine. The values in italics indicate the relative Gibbs energies and the values in bold indicate the gas-phase basicities, both in kcal mol^{-1}.

Table 3
Values of bond length (Å), bond order, ρ, in u.a., and $-\nabla^2\rho$, in u.a. for palythine neutral and protonated species

	C(7)—O(14)			O(14)—C(15)		
	Bond length	ρ	$\nabla^2\rho$	Bond length	ρ	$\nabla^2\rho$
1	1.392	0.270	−0.400	1.438	0.244	−0.472
$1H^+C(7)$	1.398	0.275	−0.568	1.448	0.231	−0.316
$1H^+C(6)$	1.276	0.340	0.144	1.479	0.204	−0.140
$1H^+N(2)$	1.371	0.281	−0.464	1.438	0.232	−0.408
$1H^+N(8)$	1.381	0.287	−0.460	1.453	0.224	−0.332

tonation. The most stable protonated species was obtained when the proton is bonded at N(2) atom whose gas-phase basicity to 249.45 kcal mol^{-1}. In contrast, the protonation at C(6) atom led to the lowest stable species (GB = 178.07 kcal mol^{-1}), with relative Gibbs energies closed to 71 kcal mol^{-1} (Fig. 3). The protonation on N(8) and C(7) led to energetically unstable species with relative Gibbs energies of 46.79 and 42.73 kcal mol^{-1}, respectively.

In order to rationalise the CH_3 radical elimination, we compared values of bond length and eletronic density (ρ_b) for all of the protonated species (Table 3, Fig. 3). The O(14)—C(15) bond length

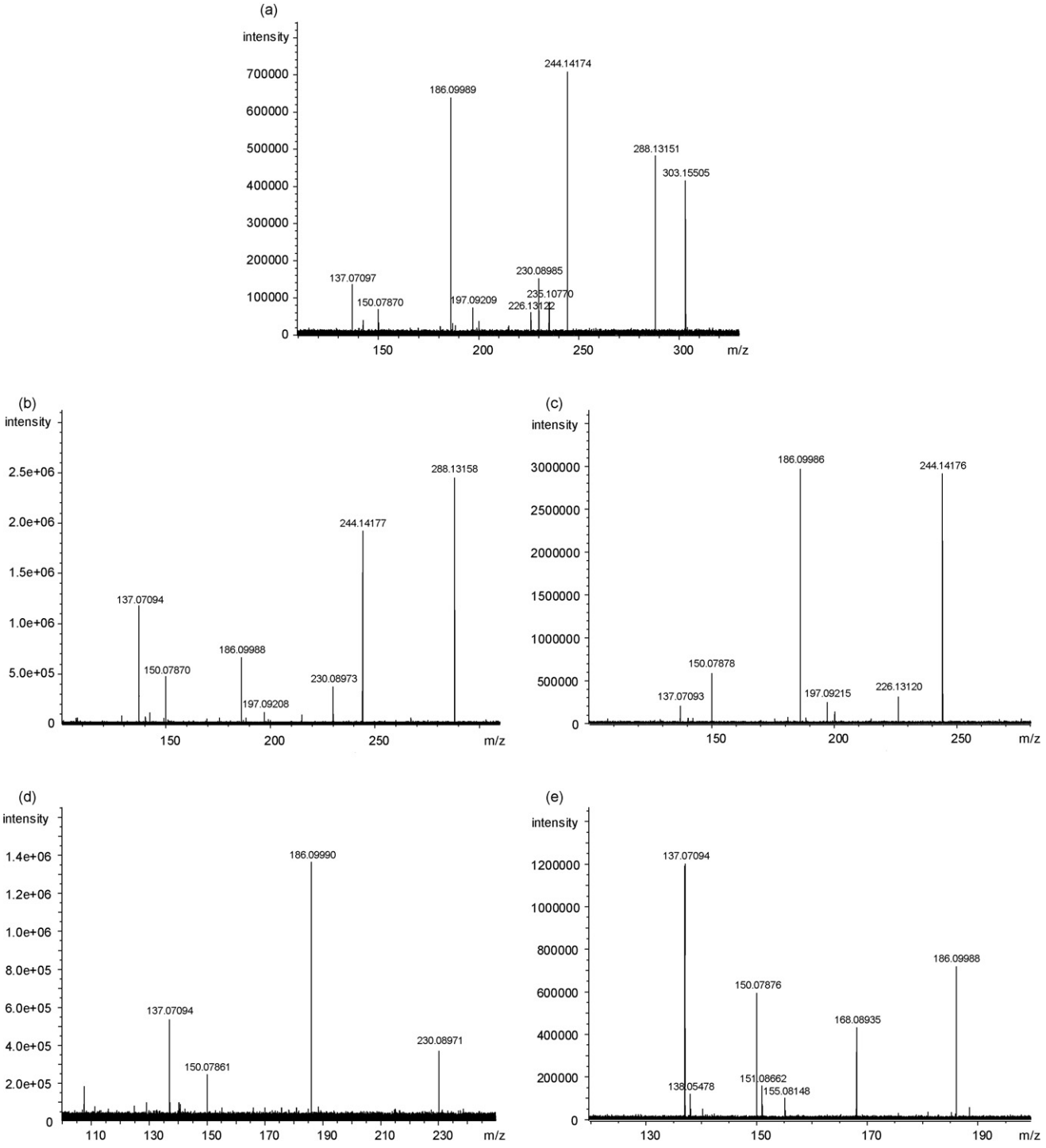

Fig. 4. The accurate-mass MS/MS and MS^3 spectra of palythinol obtained by SORI-CID–FTICR–MS^n. Spectrum(a) is the MS/MS of m/z 303, (b) is the MS^3 of m/z 288 from (a), (c) is the MS^3 of m/z 244 from (a), (d) is the MS^3 of m/z 230 from (a), (e) is the MS^3 of m/z 186 from (a).

increased after protonation which is indicative of its weakening. The C(7)—O(14) bond decreases after protonation, except when the proton is attached at C(7) atom (Table 3, Fig. 3). The 1H$^+$C(6) can be considered the most reactive protonated species, which can go on to generate the $[(M+H)\text{-}15]^+$ product ion. Moreover, this ion sustain the largest weakening at O(14)—C(15) bond, when compared to the other protonated conformers.

According to the AIM analysis of the C(7)—O(14) Bond Critical Point (BCP) in the structure (Table 3), the electron density (ρ_b) increases after protonation. It is also worth mentioning that this is evidence of the reinforcement of these bonds. As regards the O(14)—C(15) bond, values of ρ_b decrease after protonation which is indication of weakening. Thus, the protonation reforces the C(7)—O(14) bond and weakens the O(14)—C(15) bond. This effect is more pronounced for the 1 H$^+$C(6) species, because this ion has the largest value of ρ_b for C(7)—O(14) and, the lowest value for O(14)—C(15), as shown in Table 3.

As stated by AIM theory, the greater accumulation of charge in the internuclear region of a covalent bond indicates that this bond can be easily perturbed [45]. Thus, the increase in the value of $\nabla^2\rho$ for the C(7)—O(14) bond for the protonated species can be correlated with an increase in its stability.

3.2. ESI–MS/MS analysis

MS/MS analysis yielded an odd and even massed series of ions for all three MAAs analysed (Table 1 and Fig. 4). The even massed fragments are the most abundant series and are produced via the CH_3 radical elimination route. All three precursor ions are odd-massed. Even-massed ions can also be produced by loss of a nitrogen-containing neutral, but in this case this does not occur. A majority of the product ions observed are sub-fragments of the loss of the methyl radical, apart from the low abundance product ions at *m/z* 235, 199 and 197, which are produced directly from the precursor ions. It is necessary to explain here that in Scheme 1 all of the product ions occurring after the CH_3 radical elimination are represented with the charge located at the same first position necessary to for the radical elimination to occur. The square 'Z' represent a possible internal rearrange the must occur for all of these ions.

Based on Scheme 1, the Gibbs energies of fragmentation were calculated for selected product ions and the relative energy profiles elucidated (Fig. 5). The energy necessary for the CH_3 elimination to occur ($\Delta G = +35.46$ kcal mol^{-1}) is provided by the kinetic energy transferred by the collision gas. The MS^3 analyses of the fragments at *m/z* 288 and at *m/z* 186 are in agreement with the preliminary

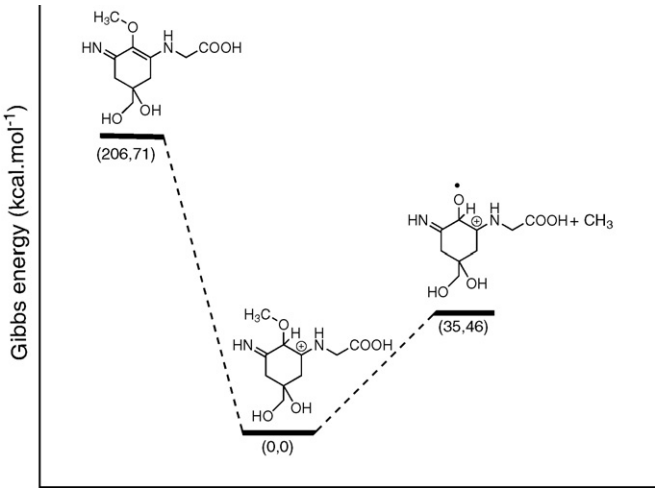

Fig. 5. Gibbs energies of fragmentation for selected product ions.

CH_3 radical elimination and also show that the odd-massed product ions at *m/z* 155, 151 and 137 were generally exceptions (see Scheme 2 and Fig. 4). The first radical cation product ions of (**2**) and (**3**) can lose, by a neutral elimination, the lateral substituent chain (pathway A, Scheme 1) to produce a product ion in common with (**1**) (*m/z* 230). A competitive fragmentation pathway (B) for (**2**) and (**3**) is also observed (Scheme 1, Table 1 and Fig. 4) with neutral elimination of CO_2 and H_2O occurring. The common ion at *m/z* 230 can also lose CO_2 and H_2O by a neutral elimination resulting in the product ion at *m/z* 168 (this ion was rarely observed in MS/MS experiments, and was only observed with good intensity in MS^3 spectra—indicative of its low stability). This ion can undergo aromatisation via a keto-enol type equilibrium, yielding an aromatic cation (Scheme 2). The charge can still be in equilibrium between the three heteroatoms, as shown in Scheme 2, pathway D. Because oxygen is the least basic atom, it is not expected to be protonated to any large degree. However, if the protonation occurs on the O atom, the aromatic radical cation can lose H_2O to produce a stable benzylic ion (*m/z* 150). In this pathway, two further routes were originally proposed leading to the formation of the product ions at *m/z* 151 and 137 by a neutral elimination of NH_3 or CH_3NH_2, respectively. These are not very good leaving groups when compared with water and the resulting product ions are also less stable than the benzylic ion. The accurate-masses of these two ions show that they have different formulae to the structures proposed and so this mechanism is in fact not occurring.

After the aromatisation of *m/z* 168, another possibility is a resonance-stabilised radical, as shown in pathway E, Scheme 2. This radical can eliminate a hydroxide radical, resulting in the very stable, highly conjugated ion at *m/z* 151 (formula confirmed by accurate-mass).

Finally, to understand the proposed formation of the product ion at *m/z* 137 (as well as *m/z* 155 and 138) we must reanalyse the same pathway before the loss of water. The ion at *m/z* 186 can undergo an internal hydrogen atom transfer (Scheme 2, pathway C) to give a carbon centered radical structure that can rearrange by proton transfer to an allylic radical [44]. Resonance of allylic radicals is well established [46], and in this case, the loss of a methoxy radical, in a process similar to that observed in EI mass spectrometry [47] can occur to produce the ion at *m/z* 155, observed with good intensity in the MS^3 spectrum. The resulting ion now behaves like a normal protonated species and confirms the existence of the pathway through the radical (pathway C). The ion at *m/z* 155 then loses either NH_3 or H_2O (depending on where the proton is located—i.e., on the relative basicities) by neutral elimination to produce the ions at *m/z* 138 and 137, respectively. The ion at *m/z* 137 is of much higher intensity than *m/z* 138 because H_2O is the better leaving group. In both of these cases, the formation of benzyl ion is the only possibility consistent with the accurate-mass data, ruling out the alternative radical route to *m/z* 137 via pathway D.

In the previous fragmentation studies of the MAAs [24], two ions (at *m/z* 235 and 197) were observed, although they were not accounted for in the fragmentation scheme proposed. The accurate-mass MS/MS spectrum (see Fig. 4) clearly shows these two peaks and the accurate-masses match to $C_{12}H_{15}N_2O_3^+$ and $C_9H_{13}N_2O_3^+$, respectively. The ion at *m/z* 197 is also observed in some of the MS^3 spectra. It is proposed that these two ions result from neutral losses and McLafferty type rearrangements (see Scheme 3). In the case *m/z* 235, there is an initial loss of water followed by a McLafferty type rearrangement within the imino-alcohol substituent, leading to the loss of methanol. There can then be a further loss of water to produce *m/z* 235. For the ion at *m/z* 197, two McLaferty type rearrangements may occur, one in the amino-acid substituent and the second in the imino-alcohol substituent. The intermediate ions are not observed in the FTICR–MS/MS analysis, but they are present as very weak product ions in the previously published triple

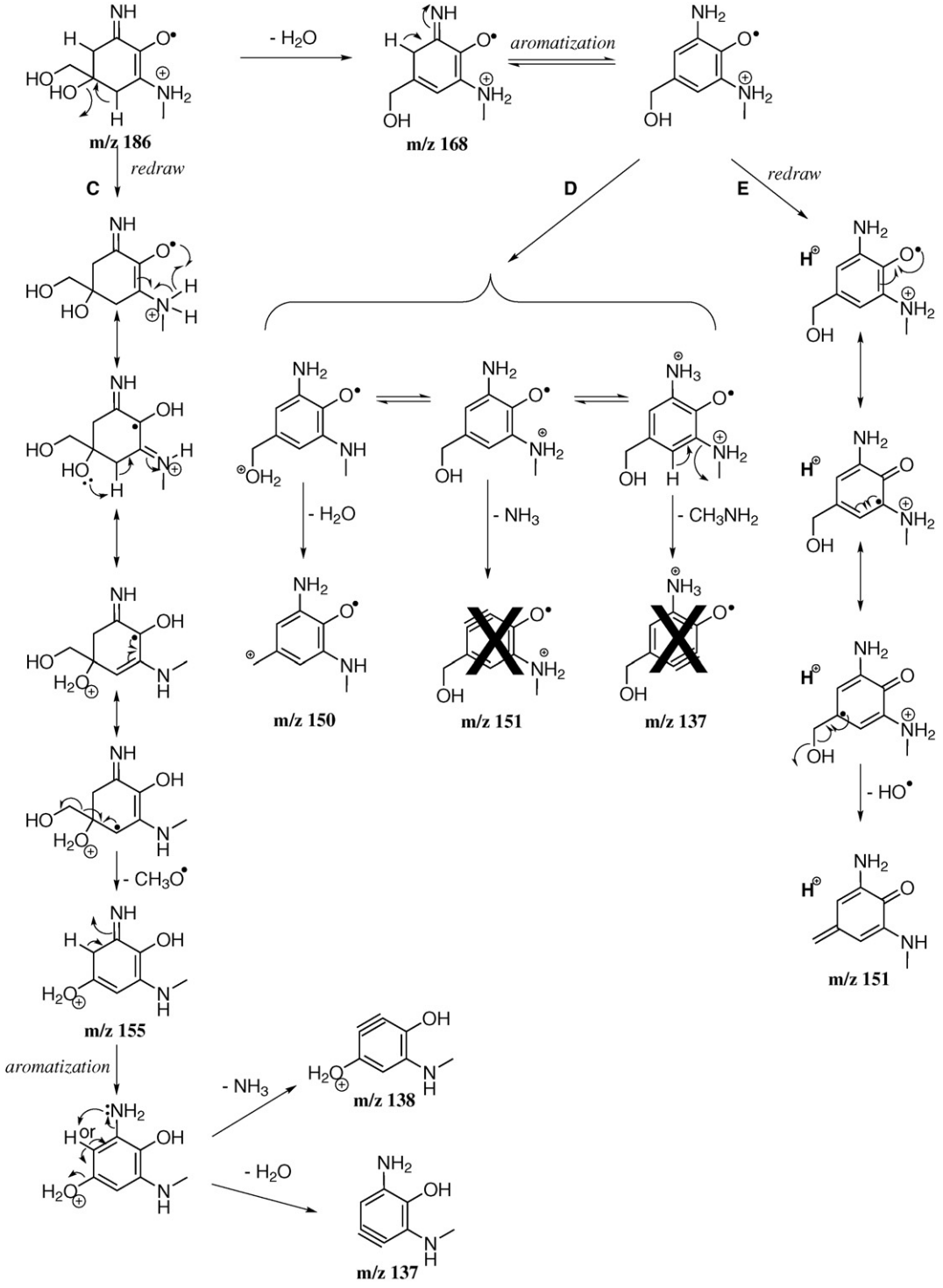

Scheme 2. The proposed mechanism for the sub-fragmentation of *m*/*z* 186 and 168 (see Scheme 1). These ions are mostly observed in the MS^3 spectrum of 186, but some are observed in other spectra.

quadrupole MS/MS study [24]. This is indicative of these fragmentation steps being rapid processes, meaning it is not possible to detect these short-lived intermediates within the time frame of the slower FTICR–MS/MS experiment. In the MS^3 of the ion at *m*/*z* 288 and 244, *m*/*z* 197 is still observed. It is proposed that, in these two cases, the radical ions can undergo a classical McLafferty rearrangement (similar to those observed in EI spectra) leading to the same product ion structure. This ion has four exchangeable protons and it is clearly observed to occur at *m*/*z* 201 in the deuterated analysis published previously [24]. Finally, from the palythinol structure, the product ion at *m*/*z* 197 can also be produced by a methyl radical cleavage followed by a concerted methanol elimination from the product ion at *m*/*z* 244, also resulting in the same molecular formula.

In all spectra, the mass accuracies are within 0.5 ppm of the theoretical masses (apart from two exceptions at 1.00 and 1.23 ppm). The mass accuracy variations across all spectra were very small, with a RMS average error of 0.05 ppm and a mean residual error of less than 0.2 ppm. The formula searches for the unknown product ions were performed with the formula of the precursor ion as the atom constraints. This lead to just one possible formula for these

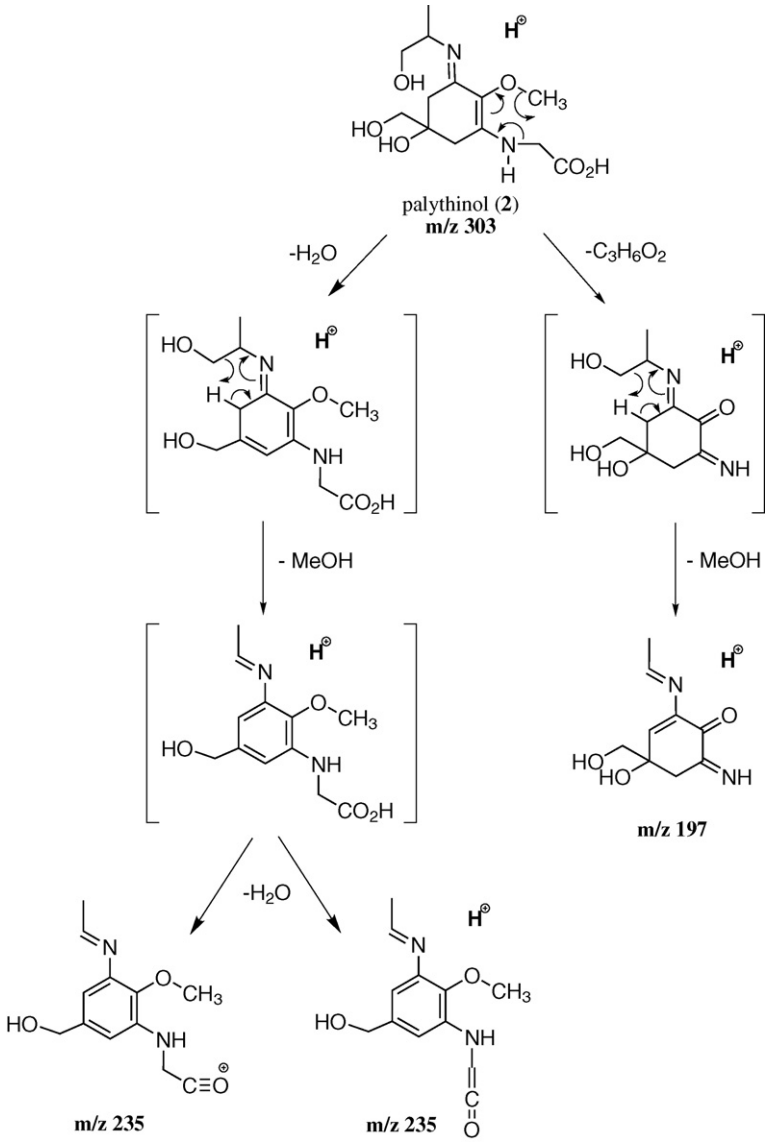

Scheme 3. The proposed mechanism of fragmentation of the protonated palythinol molecule via McLafferty-type rearrangements resulting in the ions observed at *m*/*z* 235 and 197. Analogous fragmentation is observed for the other MAAs.

ions, with a very high degree of certainty that these formulae are correct.

4. Conclusions

By analysing of theoretical parameters, bond length and eletronic density we suggest that the protonation occurs on the N(2) site and the ion $[(M+H)-15]^+$ is generated by the cleavage of the ether bond through reinforcement of the C(7)—O(14) bond and the consequent weakening of O(14)—C(15) bond. The loss of a CH_3 radical is also proven through accurate-mass data and the previously suggested loss of NH is discounted. The fragmentation of $[(M+H)-CH_3]^+$ produced a series of ions by neutral elimination and the strong influence of resonance-stabilised radical processes (similar to those that can occur in EI mass spectrometry) is clearly demonstrated in the proposed mechanism. High-resolution accurate-mass sequential mass spectrometry (FTICR–MS^n) was crucial for defining the details of this proposed mechanism and allowed us to discount several possible alternative routes. The data also confirmed the further radical losses (*m*/*z* 168–151: loss of an OH radical and *m*/*z* 186–155: loss of a CH_3O radical) that produce high stability, non-radical product ions. Finally, it was also possible to propose structures for the previously unidentified ions at *m*/*z* 235 and 197.

Acknowledgements

The authors thank FAPESP (Fundação de Amparo à Pesquisa do Estado de São Paulo, 05/01572-1, 01/13482-6 and 03/08735-8), CAPES (Coordenação de Aperfeiçoamento de Pessoal de Nível Superior), CNPq and CNPq-Millenium (Conselho Nacional de Desenvolvimento Científico e Tecnológico) and Natura for research funding and financial support.

References

[1] W.M. Bandaranayake, Nat. Prod. Rep. 15 (1998) 159.
[2] W.C. Dunlap, J.M. Shick, J. Phycol. 34 (1998) 418.
[3] R.P. Sinha, M. Klisch, A. Groniger, D.P. Hader, J. Photochem. Photobiol. B-Biol. 47 (1998) 83.
[4] J.M. Shick, W.C. Dunlap, Annu. Rev. Physiol. 64 (2002) 223.
[5] A. Groniger, R.P. Sinha, M. Klisch, D.P. Hader, J. Photochem. Photobiol. B-Biol. 58 (2000) 115.
[6] M. Klisch, D.P. Hader, J. Photochem. Photobiol. B-Biol. 55 (2000) 178.
[7] N.L. Adams, J.M. Shick, Photochem. Photobiol. 64 (1996) 149.

[8] M. Klisch, R.P. Sinha, P.R. Richter, D.-P. Hader, J. Plant Physiol. 158 (2001) 1449.
[9] T. Rezanka, M. Temina, A.G. Tolstikov, V.M. Dembitsky, Folia Microbiol. (Praha) 49 (2004) 339.
[10] W.C. Dunlap, Y. Yamamoto, Comp. Biochem. Physiol. B-Biochem. Mol. Biol. 112B (1995) 105.
[11] A. Oren, Geomicrobiol. J. 14 (1997) 231.
[12] W.M. Bandaranayake, A.D. Rocher, Mar. Biol. (Berlin) 133 (1999) 163.
[13] W.C. Dunlap, B.E. Chalker, W.M. Bandaranayake, J.J. Wu Won, Int. J. Cosmetic Sci. 20 (1998) 41.
[14] J.I. Carreto, M.O. Carignan, N.G. Montoya, Mar. Biol. (Heidelberg, Germany) 146 (2005) 237.
[15] H. Nakamura, J. Kobayashi, Y. Hirata, J. Chromatogr. 250 (1982) 113.
[16] W.C. Dunlap, B.E. Chalker, J.K. Oliver, J. Exp. Mar. Biol. Ecol. 104 (1986) 239.
[17] J.I. Carreto, M.O. Carignan, N.G. Montoya, Mar. Ecol.-Prog. Ser. 223 (2001) 49.
[18] K. Whitehead, J.I. Hedges, Mar. Chem. 80 (2002) 27.
[19] K. Whitehead, J.I. Hedges, Rapid Commun. Mass Spectrom. 17 (2003) 2133.
[20] N.P. Lopes, C.B. Stark, H. Hong, P.J. Gates, J. Staunton, Rapid Commun. Mass Spectrom. 16 (2002) 414.
[21] T. Fonseca, N.P. Lopes, P.J. Gates, J. Staunton, J. Am. Soc. Mass Spectrom. 15 (2004) 325.
[22] R. Vessecchi, P.G.B.D. Nascimento, J.N.C. Lopes, N.P. Lopes, J. Mass Spectrom. 41 (2006) 1219.
[23] X. Yang, C. Zhu, S. Cao, X. Liao, Y. Jiang, Y. Zhao, Rapid Commun. Mass Spectrom. 17 (2003) 1927.
[24] K.H.M. Cardozo, V.M. Carvalho, E. Pinto, P. Colepicolo, Rapid Commun. Mass Spectrom. 20 (2006) 253.
[25] J. Zhao, T. Shoeib, K.W.M. Siu, A.C. Hopkinson, Int. J. Mass Spectrom. 255–256 (2006) 265.
[26] R.F.W. Bader, Atoms in Molecules: A Quantum Theory, Clarendon Press/Oxford University Press, Oxford, England, 1994.
[27] M. Alcami, O. Mo, M. Yanez, J.L.M. Abboud, J. Elguero, Chem. Phys. Lett. 172 (1990) 471.
[28] J. Collen, E. Pinto, M. Pedersen, P. Colepicolo, Arch. Environ. Contam. Toxicol. 45 (2003) 337.
[29] A.D. Becke, J. Chem. Phys. 98 (1993) 5648.
[30] C. Lee, W. Yang, R.G. Parr, Phys. Rev. B: Condens. Mat. Mater. Phys. 37 (1988) 785.
[31] M.J. Frisch, G.W. Trucks, H.B. Schlegel, G.E. Scuseria, M.A. Robb, J.R. Cheeseman, V.G. Zakrzewski, J.A. Montgomery, R.E. Stratmann, J.C. Burant, S. Dapprich, J.M. Millam, A.D. Daniels, K.N. Kudin, M.C. Strain, O. Farkas, J. Tomasi, V. Barone, M. Cossi, R. Cammi, B. Mennucci, C. Pomelli, C. Adamo, S. Clifford, J. Ochterski, G.A. Petersson, P.Y. Ayala, Q. Cui, K. Morokuma, D.K. Malick, A.D. Rabuck, K. Raghavachari, J.B. Foresman, J. Cioslowski, J.V. Ortiz, B.B. Stefanov, G. Liu, A. Liashenko, P. Piskorz, I. Komaromi, R. Gomperts, R.L. Martin, D.J. Fox, T. Keith, M.A. Al-Laham, C.Y. Peng, A. Nanayakkara, C. Gonzalez, M. Challacombe, P.M.W. Gill, B.G. Johnson, W. Chen, M.W. Wong, J.L. Andres, M. Head-Gordon, E.S. Replogle, J.A. Pople, Gaussian, Inc., Pittsburgh PA. Gaussian 98, Revision A.1 (1998).
[32] E.D. Glendening, F. Weinhold, J. Comput. Chem. 19 (1998) 593.
[33] E.D. Glendening, F. Weinhold, J. Comput. Chem. 19 (1998) 610.
[34] A.E. Reed, R.B. Weinstock, F. Weinhold, J. Chem. Phys. 83 (1985) 735.
[35] A.E. Reed, L.A. Curtiss, F. Weinhold, Chem. Rev. (Washington, DC, US) 88 (1988) 899.
[36] E.D. Glendening, J.K. Badenhoop, A.E. Reed, J.E. Carpenter, J.A. Bohmann, C.M. Morales, F. Weinhold, Theoretical Chemistry Institute, University of Winsconsin, NBO 5.0, 2001.
[37] P. Popelier, Atoms in Molecules—An Introduction, Pearson Education Ltd., London, 2000.
[38] F.W. Biegler-Koenig, R.F.W. Bader, T.H. Tang, J. Comput. Chem. 3 (1982) 317.
[39] R.R. Contreras, P. Fuentealba, M. Galvan, P. Perez, Chem. Phys. Lett. 304 (1999) 405.
[40] E. Uggerud, Mass Spectrom. Rev. 26 (1992) 389.
[41] L. Random, Org. Mass Spectrom. 26 (1991) 359.
[42] M. Alcamí, O. Mó, M. Yáñez, Mass Spectrom. Ver. 20 (2001) 195.
[43] W. van Scheppingen, E. Dorrestijn, I. Arends, P. Mulder, H.G. Korth, J. Phys. Chem. A. 101 (1997) 5404.
[44] R.T. Morrison, R.T. Boyd, Organic Chemistry, third ed., Allyn & Bacon, Boston, 1973, pp. 291–292.
[45] T.S. Slee, J. Am. Chem. Soc. 108 (1986) 606.
[46] T.W. Graham Solomons, Organic Chemistry, eighth ed., Wiley and Sons, New York, 2004.
[47] F.W. McLafferty, Interpretation of mass spectra, fourth ed., University Science Books, New York, 1993.